Ab initio estimations of the isotope shift for the first three elements of the K isoelectronic sequence

Sourav Roy and Sonjoy Majumder
Department of Physics, Indian Institute of Technology-Kharagpur, Kharagpur-721302, India
(Received 27 January 2015; published 8 July 2015)

Isotope shifts (ISs) of D_1 ($ns\,^2S_{1/2} \rightarrow np\,^2P_{1/2}$) and D_2 ($ns\,^2S_{1/2} \rightarrow np\,^2P_{3/2}$) transitions for the first three elements of the K isoelectronic sequence are calculated with all-order correlated relativistic coupled-cluster theory. To get precise *ab initio* results, all the orbitals of the reference states have been optimized by a linear regression technique. Some of the important IS estimations reported here were not available in literature. Interesting features of odd-even staggering and magic neutron number effects are also observed in the case of volume shift calculations. Energy-level corrections for a few levels due to a change in the nuclear model from a point nucleus to a Fermi nucleus have been studied with interesting correlation features and compared with other theoretical results available in literature.

DOI: 10.1103/PhysRevA.92.012508 PACS number(s): 31.15.A−, 31.15.bw, 31.30.Gs, 32.10.Bi

I. INTRODUCTION

The prediction of the variation in the fine-structure constant (α) [1,2] from the quasar absorption spectra [3,4] boosts the quest among scientists to look for the right justification. The effect of this variation is estimated from the spectral shift in the frequency domain. Since the amount of shift is on the order of the isotope shift (IS) in the spectral line, the precise estimation of the IS can infer an exact variation in α in the early universe [5]. The isotopic abundances can be calculated by the technique proposed by Kozlov *et al.* [4].

The future aspect of these calculations provides a parameter for an accurate study of parity nonconservation in an atom. The parameter depends on the charge distribution inside the nucleus, and this distribution can be obtained from field shift (FS) or volume shift results of the IS [6–8]. The shifting of the energy levels due to the change in the model of the nucleus from a point type to a Fermi type [9] is a great tool to calculate the most realistic rms radius of the nucleus. Therefore a precise calculation of the volume shift can play a big role in these studies [6].

The specific mass shift (SMS) and the normal mass shift (NMS) are the other two parts of the IS. The SMS is the momentum-momentum interaction part of the electrons coming from the nuclear motion. The NMS is the reduced mass effect as we consider finite mass of the nucleus. Among these three effects, the SMS is maximally difficult to calculate as it is highly sensitive to the electron-electron correlation phenomena [10]. There have been many calculations on the isotopic shift in the past two decades, and they are based on theories, such as configuration interaction [2,4], relativistic many-body perturbation theory (MBPT) [2,4,6,11], multiconfiguration Dirac-Fock (MCDF) [12], etc. Dzuba *et al.* [6] and Berengut *et al.* [10] clearly explain the requirement of all-order methods for the SMS. Here we have performed *ab initio* calculations based on relativistic coupled-cluster (RCC) theory, which is well known as highly correlated due to its all-order character [13]. We have considered the IS in our calculations in the self-consistent (SCF) way.

Highly precise calculations of such small values in the shift requires accurate generation of the Dirac-Fock (DF) state as a reference state of the RCC calculation. We have developed a procedure to optimize all active DF orbitals using an even-tempered technique [14]. We calibrate this technique with the much-studied Mg II system and then study the isotopic shift in the D_1 and D_2 lines between various isotopes of K I, Ca II, and Sc III. Precise ISs of these elements are required for atom or ion trapping for fundamental research [15–17] as well as for astrophysical [18,19] importance. Specially, Sc III is of recent interest [20,21], but no IS values are available in literature to our knowledge. We also study level corrections and corresponding correlation effects on them along with the mass shift constants for the D_1 and D_2 lines and shift constants for individual energy levels too. The effect of variation in the numbers of neutrons and protons on the IS of the D_1, D_2 transition are analyzed.

Lack of *ab initio* many-body calculations on the IS of K-like systems motivates us to perform these correlation exhaustive calculations. It is more realistic to consider the electrons and nucleus actual mass in the NMS calculations in place of the reduced mass of the electrons as explained in the literature [2,22]. So we calculate the NMS effects in full *ab initio* technique as is considered for SMS and FS calculations. As the relativistic corrections of the IS are very small for light atoms [2], such as K I and Ca II, we do not consider this correction in our present calculations.

II. THEORY

A. Isotope shift matrix elements and implementation

The atomic Dirac-Coulomb Hamiltonian can be written as

$$H = \sum_{i=1}^{N} [c\vec{\alpha}_i \cdot \vec{p}_i + (\beta_i - 1)mc^2 + V_{\rm nuc}(r_i)] + \sum_{i<j}^{N} \frac{1}{r_{ij}}, \quad (1)$$

where usual notations are used [23]. Now we add three extra terms in this Hamiltonian for the isotope shift. Among them, the most computationally difficult term is the SMS, which is a two-body operator [24],

$$\frac{1}{2M} \sum_{i<j}^{N} \vec{p}_i \cdot \vec{p}_j. \quad (2)$$

Here, $\vec{p}_i$ and M are the momentum of the "i"th electron and mass of the nucleus, respectively. N is the total number of

interacting electrons. In the program, we add the matrix element of this part with the Coulomb interaction in an appropriate way. The other two parts of the IS, NMS, and FS, have a one-body form of operators and have been considered along with the one-body part of Eq. (1). The NMS operator has the form of

$$\frac{1}{2M}\sum_{i}^{N}\vec{p}_i\cdot\vec{p}_i. \tag{3}$$

The field shift δE can be written as

$$\delta E = F\delta\langle r^2\rangle, \tag{4}$$

where F is the field shift parameter and $\delta\langle r^2\rangle$ is the change in root-mean-square radius [24].

The specific mass shift constant $K_{\rm SMS}$ and normal mass shift constant $K_{\rm NMS}$ can be calculated from the energy shift by multiplying them with the nuclear mass,

$$K_{\rm MS} = M\langle j_a m_{j_a}|H_{\rm MS}|j_b m_{j_b}\rangle, \tag{5}$$

where $K_{\rm MS} = K_{\rm NMS} + K_{\rm SMS}$ and $H_{\rm MS} = H_{\rm NMS} + H_{\rm SMS}$.

We have calculated the single valence reference wave function Φ_v, having a valence electron at the "v"th orbital, at the DF level using the basis set expansion technique [25]. The actual atomic state Ψ_v in the RCC theory can be expressed as

$$\Psi_v = e^T\{1+S_v\}\Phi_v. \tag{6}$$

Here, T and S_v are the excitation cluster operators [23] for core only and core-valence orbitals, respectively. The matrix elements for the Dirac-Coulomb-Breit Hamiltonian have been discussed in our earlier papers [13,23]. Although the matrix elements of different parts of the IS are discussed in many references, such as Refs. [12,22], we discuss them here for the completeness of the paper.

Now the actual matrix element of the nonrelativistic SMS part is

$$\frac{1}{2M}\sum_{i<j}\langle ab|\vec{p}_i\cdot\vec{p}_j|cd\rangle = \frac{1}{2M}\sum_{i<j}\sum_{q=-1}^{1}\begin{pmatrix} m_a & 1 & j_c \\ j_a & q & m_c\end{pmatrix}\times\begin{pmatrix} m_b & q & j_d \\ j_b & 1 & m_d\end{pmatrix}X^1(abcd), \tag{7}$$

where the effective interaction strength is

$$X^1(abcd) = -\langle a\|\vec{p}_i^{\,1}\|c\rangle\langle b\|\vec{p}_j^{\,1}\|d\rangle. \tag{8}$$

Each of these reduced matrix elements on the right-hand side of Eq. (8) can be written as the multiplication of an angular part and the radial Vinti integral [26,27],

$$\begin{aligned}&\langle a\|\vec{p}^{\,1}\|b\rangle \\ &= -i\langle a\|C^1\|b\rangle\Bigg[\int_0^\infty P_a(r)\\ &\quad\times\left(\frac{d}{dr}-\frac{\kappa_a(\kappa_a+1)-\kappa_b(\kappa_b+1)}{2r}\right)P_b(r)dr\\ &\quad+\int_0^\infty Q_a(r)\left(\frac{d}{dr}-\frac{-\kappa_a(-\kappa_a+1)+\kappa_b(-\kappa_b+1)}{2r}\right)\\ &\quad\times Q_b(r)dr\Bigg].\end{aligned} \tag{9}$$

The triangular and parity selection rules [28] govern the total environment of the matrix element.

NMS is an operator of rank zero. The actual matrix element of it can be written with the help of the Wigner-Eckart theorem as

$$\langle j_a m_{j_a}|H_{\rm NMS}|j_b m_{j_b}\rangle = (-1)^{j_a-m_{j_a}}\begin{pmatrix} j_a & 0 & j_b \\ m_{j_a} & 0 & m_{j_b}\end{pmatrix}\times\langle j_a m_{j_a}\|H_{\rm NMS}\|j_b m_{j_b}\rangle\delta(j_a,j_b), \tag{10}$$

and the reduced matrix element has the form

$$\langle j_a m_{j_a}\|H_{\rm NMS}\|j_b m_{j_b}\rangle = (-1)^{j_a+1/2}[j_a,j_b]\times\begin{pmatrix} j_a & 0 & j_b \\ 1/2 & 0 & -1/2\end{pmatrix}R_{\rm NMS}, \tag{11}$$

where $[j_a,j_b]=\sqrt{(2j_a+1)(2j_b+1)}$ and $R_{\rm NMS}$ is the radial part of the matrix element. Now from the above Eqs. (9) and (10), one can easily derive that

$$\langle j_a m_{j_a}|H_{\rm NMS}|j_b m_{j_b}\rangle = R_{\rm NMS}. \tag{12}$$

Therefore, the matrix element for the NMS has no angular part. Now,

$$\langle a|H_{\rm NMS}|b\rangle = \frac{1}{2M}\sum_i\langle a|\vec{p}_i^{\,2}|b\rangle. \tag{13}$$

A useful form of this matrix element derived from the relation $\vec{p}^{\,2} = -(\frac{\partial}{\partial r})^2 + \frac{l(l+1)}{r^2}$ [12] is

$$\langle a|\vec{p}^{\,2}|b\rangle = \int_0^\infty\left(\frac{\partial P_a}{\partial r}\frac{\partial P_b}{\partial r}+\frac{\partial Q_a}{\partial r}\frac{\partial Q_b}{\partial r}+\frac{l_b(l_b+1)P_aP_b+\tilde{l}_b(\tilde{l}_b+1)Q_aQ_b}{r^2}\right)dr, \tag{14}$$

where $\tilde{l}=2j-1$.

We consider the mass of the nucleus in atomic units and convert the energy shift in gigahertz units by multiplying with the conversion factor $6.579\,66\times10^6$.

However, the NMS of a transition between two isotopes A and A' can also be calculated [24] proximately with the help of the simple equation given below,

$$\Delta E_{\rm NMS}^{A,A'} = \Delta E^{1,2}\left(\frac{1}{\mu_A}-\frac{1}{\mu_{A'}}\right), \tag{15}$$

where $\Delta E^{1,2}$ is the actual energy difference between state 1 and state 2 and μ is the reduced mass of the system.

For the field shift calculation the nucleons are considered having Fermi-type distributions [9], such as

$$\rho_{\rm Fermi}^{\rm nuc}(r) = \frac{\rho_0}{1+e^{(r-c)/a}}, \tag{16}$$

where parameter a is related with the nuclear skin thickness t as $a = t/4\ \ln 3$. The value of skin thickness parameter t is taken as 2.30 fm [9]. The parameter c is the half density radius, which is related with the mean-square radius as

$$\langle r^2\rangle \approx \tfrac{3}{5}c^2+\tfrac{5}{7}\pi^2a^2. \tag{17}$$

We calculate the rms radius of the nucleus using the empirical formula [29],

$$\sqrt{(\langle r^2\rangle)} = 0.836A^{1/3}+0.570\ \text{fm}, \tag{18}$$

where A is the mass number.

B. Optimization of the Gaussian type of orbitals

The magnitude of the IS is very small in comparison to the DC Hamiltonian given in Eq. (1). Therefore, the accuracies of the wave functions are one of the most important criteria in IS calculations. Astutely we take special care to generate the Gaussian type of orbital- (GTO-) based wave functions for the reference state (DF state) of the RCC theory. We apply an iterative procedure to optimize all the active orbitals of particular spin-orbit symmetry and obtain the best possible even-tempered exponents for the GTO basis.

1. Iterative procedure

We started with a universal basis (UB) of GTO [30] type. Our target is to obtain the best values of the parameters α_0 and β for each symmetry such that the GTO wave functions over radial parameters mostly agree with the DF wave functions obtained using a sophisticated numerical approach GRASP92 [31].

Let us consider that ϕ_{ij} is one of the elements of the GTO basis set, where i stands for a particular symmetry and j is the basis index in that symmetry. We have chosen orbitals for optimization in such a way that it covers all the active bound orbitals (including all cores) of the particular symmetry. Initially, we consider the universal values of the exponent parameters, say ($\alpha_0^{(0)} = 0.005\,25$, $\beta^{(0)} = 2.73$) for all symmetries.

Step 1. The optimization has been started from $i = 1$ (i.e., s symmetry). The orbital energies, expectation values of r and $1/r$ (i.e., $\langle r\rangle$ and $\langle 1/r\rangle$, respectively) are calculated with respect to orbital wave functions obtained from the GTO basis and GRASP92. The global minimum of the deviation between the two results and keeping the old value of α_0 have been searched by varying β first with step size 0.02. Once we get the optimum value of β, we start the optimization of α in a similar way. The value of α_0 has been changed with an interval of 0.0005 on either side of the universal value 0.005 25 until its optimum value is achieved. The differences for suitably chosen DF active orbitals are fitted by a straight line using a linear regression approach. This fitting is performed for each pair of exponents and finds the exponent pair corresponding to the minimum slope for that symmetry. At this step, exponent parameters of other symmetries are considered as UB exponents. In Fig. 1, the convergence of the regression procedure for the s symmetry of Mg II has been shown with three iterations (initial, intermediate, and final) using one core and four virtual orbitals. In this procedure $\langle 1/r\rangle$ data points are placed close to the origin so that variations in this matrix element have a maximal effect on the slope. By using these arrangements of matrix elements along the x axis we get the best agreement for DF wave functions with the GRASP92 results in the nuclear vicinity, which is necessary for an accurate calculation of the isotope shift. The final iteration yields the best parameter pair named $(\alpha_0^{(1)},\beta^{(1)})_{i=1}$.

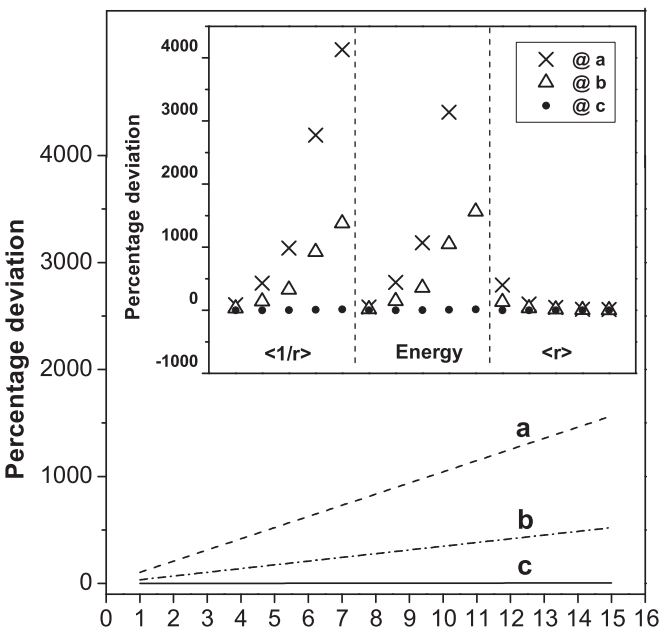

FIG. 1. Three steps of iteration ("*a*," "*b*," and "*c*") of the optimization technique for five orbitals of the s symmetry of Mg II are shown here. The data points shown in the inset are the percentage deviation of the three different DF matrix elements ($\langle 1/r\rangle$, $\langle r\rangle$, and $\langle H\rangle$) evaluated using GTO wave functions from the corresponding results using GRASP92. The serial number considered along the x axis of the main plot (linear regression curve a, b, or c) represents the above 15 data points at each level of iteration.

TABLE I. Comparison of the IS with experimental results of Mg II for the transition $3s\,^2S_{1/2} \rightarrow 3p\,^2P_{3/2}$ (D_2). All data are given in gigahertz units. The experimental value for the D_2 line of shift ^{26,24}Mg = 3.050(±0.1)[a] GHz and a semiempirical accurate calculation of ^{26,25}Mg = 1.461(±0.1)[a] GHz.

Test no.	$(N,n_{\rm sym})$	Isotopes	NMS	FS	SMS	Total	Scaling of SMS
1	93,7	^{26,25}Mg	0.920	−0.023	0.392	1.289	1.439
		^{26,24}Mg	1.906	−0.046	0.886	2.746	1.343
2	100,7	^{26,25}Mg	0.930	−0.023	0.495	1.402	1.119
		^{26,24}Mg	1.928	−0.047	1.121	3.002	1.043
3	105,7	^{26,25}Mg	0.928	−0.024	0.556	1.460	1.002
		^{26,24}Mg	1.924	−0.047	1.162	3.039	1.009

[a]Drullinger *et al.* [32]. N: The number of active orbitals. $n_{\rm sym}$: The number of symmetry. (α_0,β) = (0.0025, 1.85); (0.0011, 1.63); (0.0009, 1.71); (0.0005, 1.65); (0.0005, 1.65); (0.0009, 1.65); (0.0009, 1.65) for $S_{1/2}$, $P_{1/2}$, $P_{3/2}$, $D_{3/2}$, $D_{5/2}$, $F_{5/2}$, and $F_{7/2}$, respectively.

Step 2. As explained in Step 1, the best pair of exponent parameters for $i = 2$ ($P_{1/2}$ symmetry) are evaluated. Here we choose exponent parameters as $(\alpha_0^{(1)},\beta^{(1)})_i$ for orbitals of i=1 symmetry and $(\alpha_0^{(0)},\beta^{(0)})_i$ for the rest of the symmetries ($i > 2$).

Step 3. We proceed in the same way as for other symmetries and get the complete set of optimized exponent parameters at the first iteration level, i.e., $(\alpha_0^{(1)},\beta^{(1)})_i$ for all i.

TABLE II. D_1 transitional isotopic shift between different isotopes of Mg II; all values are given in gigahertz units.

	$3s\,^2S_{1/2} \rightarrow 3p\,^2P_{1/2}$				
		NMS			
Isotopes	SMS	*Ab initio*	Numerical	FS	Total
$A^{25,26}$	0.556	0.924	0.902	−0.023	1.457
$A^{24,26}$	1.160	1.858	1.880	−0.047	2.963

TABLE III. D_1 and D_2 transitional isotopic shifts between different isotopes of K I; all values are given in megahertz units.

	SMS		NMS		FS		Total	
Isotopes	CC	Others	CC	Others	CC	Others	CC	Expt.
			$4s\ ^2S_{1/2} \rightarrow 4p\ ^2P_{1/2}$					
^{38,39}K	19.41		−153.09		6.32		−127.36	−127.0(53)[a]
^{40,39}K	−19.47		146.27		−5.92		120.88	125.58(26)[b]
								125.46(10)[e]
^{41,39}K	−37.24	–32(21)[c]	286.35	267[c]	−12.44	–13(5)[c]	236.67	235.25(75)[a]
		–62.1[d]				–12.9[d]		235.27(33)[b]
								235.49(9)[e]
^{42,39}K	−54.56		419.13		−19.28		345.29	351.7(19)[a]
^{43,39}K	−72.31		545.97		−26.32		447.34	459.0(12)[a]
			$4s\ ^2S_{1/2} \rightarrow 4p\ ^2P_{3/2}$					
^{38,39}K	22.31		−155.87		6.12		−127.44	
^{40,39}K	−22.37		148.30		−6.12		119.81	126.43(30)[b]
								126.03(15)[e]
^{41,39}K	−42.64	–62.5[d]	290.00		−12.50	–12.9[d]	234.86	236.15(37)[b]
								236.18(17)[e]
^{42,39}K	−62.31		425.17		−19.41		343.45	
^{43,39}K	−82.96		556.73		−26.52		447.25	

[a]Touchard *et al.* [37].
[b]Bendali *et al.* [38].
[c]Berengut *et al.* [10].
[d]Safronova and Johnson [11].
[e]Falke *et al.* [39].

Step 4. We repeat the method from Step 1 to Step 3 with the updated exponent parameters for each symmetry until we get a minimum slope for all the considered orbitals of all the symmetries. This regression analysis yields optimized exponents of the even-tempered basis for all the symmetries. The calculated DF wave functions using this basis set have remarkable agreement with the corresponding wave functions obtained from GRASP92 throughout the radial extent.

2. *Testing of optimization in the IS with* Mg II

We would like to apply the optimized GTO wave functions in the RCC calculation of the IS for Mg II, which has been estimated several times in literature for theoretical and as well as experimental endeavors [1,26,32–36]. Mg II is a simple single valence system that has 11 electrons but has enough electrons for a correlation study. Experimental values of the IS for the D_2 lines of Mg II are available in literature [32], which we consider for calibration. Table I represents the results of four different tests with respect to the parameters of the basis for the SMS, NMS, and FS contributions in the total IS.

In the RCC calculation, atomic DF orbitals for all the symmetries are considered within a reasonable energy range including all cores. Here we show the improvement in the SMS values as we improve GTO-DF orbitals. In Table I, we begin the IS results obtained from the GTO-DF orbitals using the UB basis, and the initial step of optimization value calculated with this basis needs a scaling factor of 0.466 so that our calculated total values of the ISs agree with experiment [32]. But our target is to get precise results using *ab initio* calculation (i.e., without any scaling factor). Therefore we use optimized DF orbitals for further tests. As we know among the three parts of the IS, the SMS is very sensitive to the many-body correlation effect. Therefore we systematically increase the number of total active orbitals to the numerical convergence of the SMS values. On the process of increasing the number of active orbitals, Table I shows how the scaling factor for the SMS improves. Finally we get a converged SMS for ^{26,25}Mg that is 0.556 GHz and for ^{26,24}Mg that is 1.162. Berengut *et al.* got a similar value of the SMS [1.196(0.018) GHz] for ^{26,24}Mg [10]. The numerical calculation of the NMS shift for the D_2 line of ^{26,24}Mg with NIST energy values yields 1.881 GHz whereas our *ab initio* calculation estimates 1.924 GHz. Burenget *et al.* [10] got 1.185 GHz by numerical procedure. However, their other NMS results agree well with the NIST results. Most likely, this particular NMS value perhaps was not estimated correctly. Also, their calculated FS value for this transition is −0.042 GHz and is in good agreement with our calculated value of −0.047 GHz. The experimental value for ^{26,24}Mg had been measured by Drullinger *et al.* from the Doppler-free spectra of natural Mg II isotopes [32], although their results for ^{26,25}Mg had been calculated with the help of a semiempirical procedure.

Table II represents the IS of the D_1 line of Mg II for isotopes ^{24}Mg, ^{25}Mg, and ^{26}Mg. Numerically calculated [Eq. (15)] NMS values are shown in column 4, and the *ab initio* results of the NMS are given in column 3. Although there is no experimental result for the D_1 line in literature to comment on accuracy, we do see consistency of our presented results with the D_2 lines presented in Table I.

III. RESULTS AND DISCUSSIONS

We present the IS data for the D_1 and D_2 transition lines of K I, Ca II (^{A,40}Ca), Ca II (^{A,44}Ca), and Sc II in Tables III–VI,

TABLE IV. D_1 and D_2 transitional isotopic shifts among different isotopes of Ca II; all values are given in megahertz units.

	SMS		NMS		FS		Total	
Isotopes	CC	Others	CC	Others	CC	Others	CC	Expt.
			$4s\,^2S_{1/2} \rightarrow 4p\,^2P_{1/2}$					
^{39,40}Ca	−19.0		−289.2		44.2		−263.9	
^{41,40}Ca	19.1		276.8		−43.5		252.4	
^{42,40}Ca	35.9		539.2		−86.5		488.6	436.2(22.8)[b]
								468[d]
^{43,40}Ca	50.1	22(1)[e]	788.7	723[e]	−129.7	−36(3)[e]	709.1	706(42)[a]
		−96[f]				−36[f]		684.7(36.3)[b]
^{44,40}Ca	65.6		1027.6		−172.8		920.4	842(3)[c]
								839.4(14.7)[b]
^{45,40}Ca	83.9		1257.6		−215.2		1126.3	
^{46,40}Ca	98.3		1473.7		−257.1		1314.9	1256.7(35.7)[b]
^{47,40}Ca	111.6		1689.3		−298.4		1502.5	
^{48,40}Ca	125.3		1892.9		−340.5		1677.6	1758.0(24.0)[b]
			$4s\,^2S_{1/2} \rightarrow 4p\,^2P_{3/2}$					
^{39,40}Ca	−21.2		−293.9		44.1		−271.0	
^{41,40}Ca	20.2		281.6		−43.6		258.2	
^{42,40}Ca	38.7		548.1		−86.7		500.1	436.2(22.8)[b]
^{43,40}Ca	53.1	−5(1)[e]	801.6	729[e]	−129.8	−36(3)[e]	724.9	713(31),[a]
		−101[f]				−36[f]		684.7(36.3)[b]
^{44,40}Ca	71.1		1043.5		−173.1		941.5	842(13),[c]
								839.4(14.7)[b]
^{45,40}Ca	91.0		1278.4		−215.4		1154.0	
^{46,40}Ca	106.6		1501.3		−257.5		1350.4	1256.7(35.7)[b]
^{47,40}Ca	121.3		1715.3		−298.7		1537.9	
^{48,40}Ca	136.3		1924.3		−341.0		1719.6	1758.0(24.0)[b]

[a]Kurth *et al.* [42].
[b]Maleki and Goble [40].
[c]Mårtensson-Pendrill *et al.* [41].
[d]Bruch *et al.* [57].
[e]Berengut *et al.* [10].
[f]Safronova and Johnson [11].

respectively. The corresponding available experimental results are also compared. Our calculated FS, SMS, and NMS are also shown separately in each table to study the variations in results among different calculations as well as their individual contributions to the total IS. For all three species, the NMS contribution is maximum, and it decreases with the increasing nuclear mass, but no such regular trend has been observed for the FS and SMS.

In Table III, the most stable isotope of potassium ^{39}K is taken as a reference, and the shifts with ^{38,40,41,42,43}K are estimated. Our calculated total IS values are in good agreement ($\sim$0.6% for the D_1 line and $\sim$0.5% for the D_2 line) with the experiments by Touchard *et al.* [37], Bendali *et al.* [38], and Falke *et al.* [39] for $K^{41,39}$ transitions. The maximum discrepancies around 3.7% and 5% arise for the D_1 and D_2 lines, respectively, for the transition $K^{40,39}$. Safronova and Johnson performed the calculations of the IS for $K^{40,39}$ using the MBPT method up to a third-order correlation correction [11]. Berengut *et al.* performed SCF-Hartree-Fock calculations along with a few orders of correlation [10]. Our RCC results for the SMS and FS are in good agreement with the calculations by Berengut *et al.*, but significant differences have been observed in the case of the NMS value. This is due to their numerical approach of their NMS evaluation, whereas we use a fully *ab initio* technique. Furthermore, to mention that numerical calculation of the NMS with our calculated excitation energies yields 266 MHz, which is very close to their calculated 267-MHz value.

In Table IV, we present the IS results referred to the isotope ^{40}Ca along with the experimental results for comparison. Our results show little disagreement with the measurements of Maleki and Goble [40] using a Fabry-Pérot interferometer and Mårtensson-Pendrill *et al.* [41] using fast-ion beam collinear laser spectroscopy; discrepancies are around 6% and 7%, respectively. But we get very good agreement with the latest experiment by Kurth *et al.* (discrepancies of $\sim$0.4% for D_1 and 1.7% for D_2) using "dark resonance" generated between ground and excited states [42]. The results of ^{43,40}Ca are also compared with calculations by Berengut *et al.* [10] and Safronova and Johnson [11]. In the case of the D_1 and D_2 lines of ^{43,40}Ca, significant correlation effects are observed due to which we obtain positive SMS contributions, whereas Safronova and Johnson got negative contributions for the D_1 and D_2 transitions. The consistency of the SMS contributions and the nature of the increment of the values for both of these transitions from Safronova and Johnson

TABLE V. D_1 and D_2 transitional isotopic shifts among different isotopes of Ca II; all values are given in megahertz units.

Isotopes	SMS	NMS	FS	Total CC	Total Expt.
		$4s\ ^2S_{1/2} \rightarrow 4p\ ^2P_{1/2}$			
^{39,44}Ca	−86.6	−1320.1	217.1	−1189.6	
^{41,44}Ca	−48.6	−754.8	129.4	−674.0	
^{42,44}Ca	−31.7	−491.2	86.3	−436.6	−417(3)[a]
^{43,44}Ca	−15.1	−240.3	43.1	−212.3	−170(8)[a]
^{45,44}Ca	16.3	230.1	−42.3	204.1	249(3)[a]
^{46,44}Ca	31.7	450.9	−84.3	398.3	445.2(0.6)[a]
^{47,44}Ca	44.9	660.3	−125.6	579.6	
^{48,44}Ca	57.6	861.8	−167.7	751.7	854(3)[a]
		$4s\ ^2S_{1/2} \rightarrow 4p\ ^2P_{3/2}$			
^{39,44}Ca	−94.6	−1343.0	217.2	−1220.4	
^{41,44}Ca	−53.2	−767.4	129.5	−691.1	
^{42,44}Ca	−34.7	−497.4	86.4	−445.7	−412(12)[a]
^{43,44}Ca	−15.5	−246.1	43.3	−218.3	−165(14)[a]
^{45,44}Ca	17.6	234.0	−42.3	209.3	
^{46,44}Ca	33.2	457.1	−84.4	405.9	450(13)[a]
^{47,44}Ca	47.8	671.4	−125.6	593.6	
^{48,44}Ca	62.8	875.3	−167.9	770.2	857(14)[a]

[a]Mårtensson-Pendrill *et al.* [41].

to Berengut *et al.* and then from Berengut *et al.* to ours can be justified only due to improvement in correlation considered in the respective calculations. Little differences of their results from ours in the NMS values reveal once again the discrepancies between the numerical and the *ab initio* techniques. Discrepancies in the FS results are also seen here due to improved correlation calculations.

Most of the available works [40,43,44] in literature of the IS for Ca II have considered the ^{40}Ca isotope as a reference, but a few groups, such as Mårtensson-Pendrill *et al.* considered ^{44}Ca as a reference due to experimental advantage [41]. In Table V, comparisons of our calculated results with reference to the ^{44}Ca isotope have been made with the experimental results of Mårtensson-Pendrill *et al.* We see a significant difference between the two results. As we will see in the other tables and

TABLE VI. D_1 and D_2 transitional isotopic shifts among different isotopes of Sc III; all values are given in gigahertz units.

Isotopes	SMS	NMS	FS	Total
		$4s\ ^2S_{1/2} \rightarrow 4p\ ^2P_{1/2}$		
^{41,45}Sc	512.0	1450.8	−136.9	1825.9
^{43,45}Sc	244.1	691.9	−70.5	865.5
^{44,45}Sc	119.2	337.8	−35.9	421.1
^{46,45}Sc	−114.9	−324.4	36.2	−403.1
^{47,45}Sc	−224.3	−633.8	73.1	−785.0
		$4s\ ^2S_{1/2} \rightarrow 4p\ ^2P_{3/2}$		
^{41,45}Sc	560.1	1515.2	−137.1	1938.2
^{43,45}Sc	266.9	722.6	−70.4	879.1
^{44,45}Sc	130.5	352.7	−35.9	447.3
^{46,45}Sc	−126.0	−338.6	36.4	−428.2
^{47,45}Sc	−245.4	−661.9	73.3	−834.0

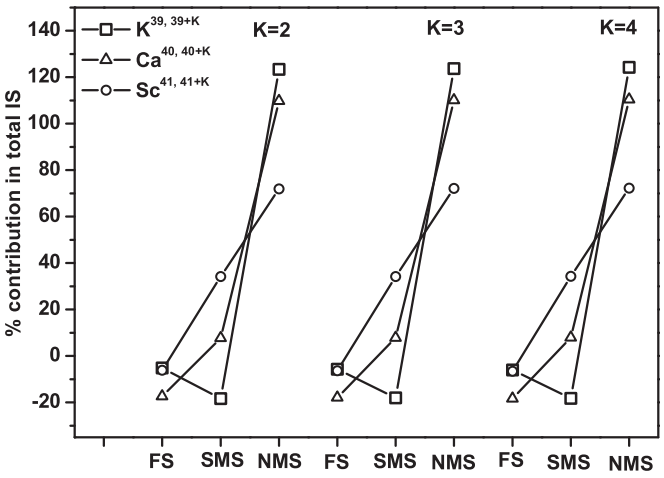

FIG. 2. Effects of proton number variation in the nucleus on the percent contribution of the FS, SMS, and NMS in the total isotopic shift in the D_2 lines. Reference neutron numbers are kept at 20 for all species.

figures in this paper our calculations yield a precise value of the IS parameters with the correct trends of the SMS, NMS, and FS of individual states of Ca II. Also, because all three contributions as well as the total IS show systematic changes with respect to a change in the difference of neutron numbers, it would be worthy to consider re-investigating the experiment. A similar trend has been observed in K I and Sc III also.

In Table VI the shifts are calculated from the most abundant isotope ^{45}Sc to some of other stable isotopes ^{41,43,44,46,47}Sc, though none of them are found in literature to compare.

We can also examine the proton number effects on the IS by comparing the data of the D_1 and D_2 lines of the isoelectronic sequence of K I. The percent contributions of the FS, SMS, and NMS to the total IS for the D_2 lines from the same neutron number of the species are depicted graphically in Fig. 2. For the D_1 line, similar effects have been observed and are not shown in the paper separately. There are three sets of data for the D_2 line shifts, shown in Fig. 2, with respect to neutron number change K ($K = 2$–4). Each set contains values of effects for all three species K I, Ca II, and Sc III. The IS shift of the D_2 transitions of each species in a particular set are chosen in such a way that the relation between the contributions of the FS, NMS, and SMS over the isoelectronic sequence can be studied. It is clear from Fig. 2 that with the increase in proton number, the percent contribution of the FS and NMS are decreasing whereas the percent contributions of the SMS are increasing. Interestingly the changes from Sc III to Ca II and from Ca II to K I are almost the same, about 23%. The most interesting feature occurs for the FS contributions. The percent contributions of the FS of Sc III is a little larger than K I (K I $\sim -8\%$, Sc III $\sim -8.5\%$) for all the sets, but for Ca II it is $\sim -20\%$. Please note that it is expected from the above trends that the FS contribution for Ca II should lie in between the contributions for K I and Sc III due to their positions in the periodic table. The presence of a proton magic number in the reference isotope of ^{40}Ca II is responsible for this unusual behavior. The variation in nuclear volume between one reference isotope to the others is the largest for Ca although the neutron number difference is the same for all of the species.

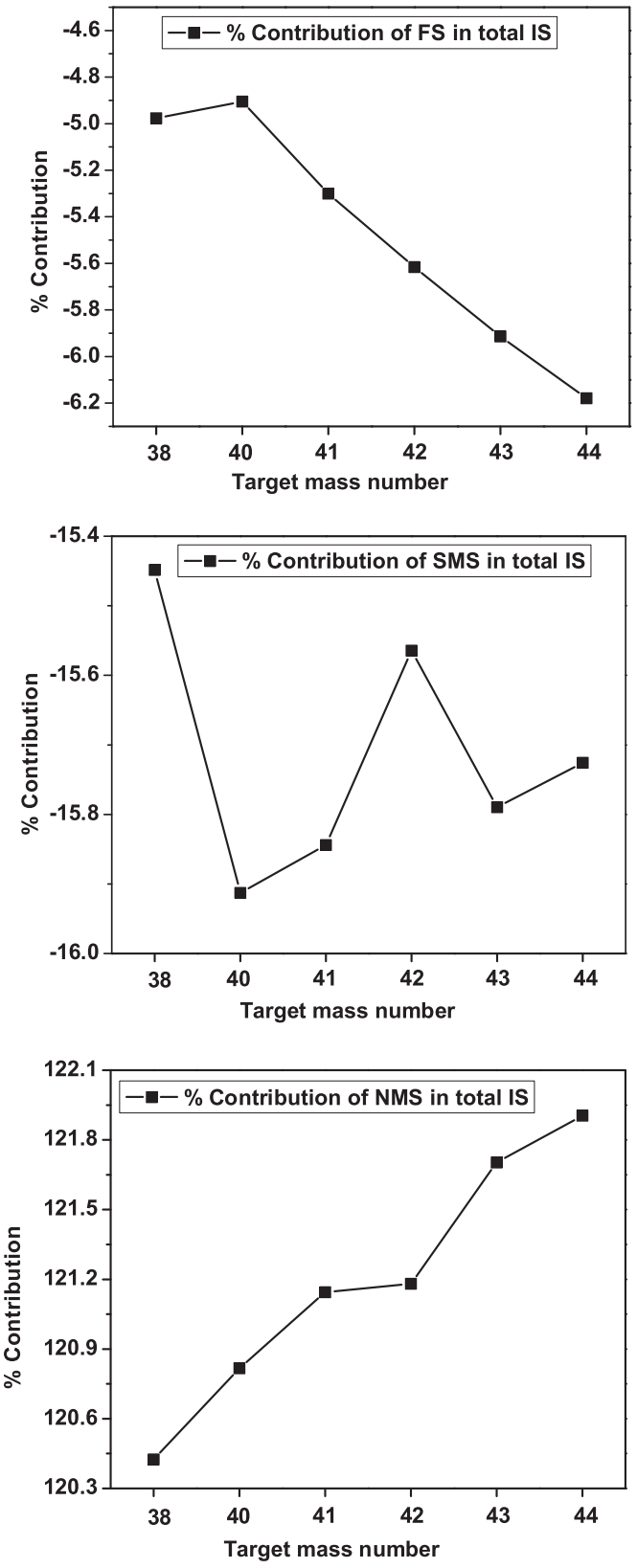

FIG. 3. Effects of the change in neutron numbers on the percent contribution of the FS, SMS, and NMS in the total isotopic shift for the D_2 line of K I. Here the reference isotope is K^{39}.

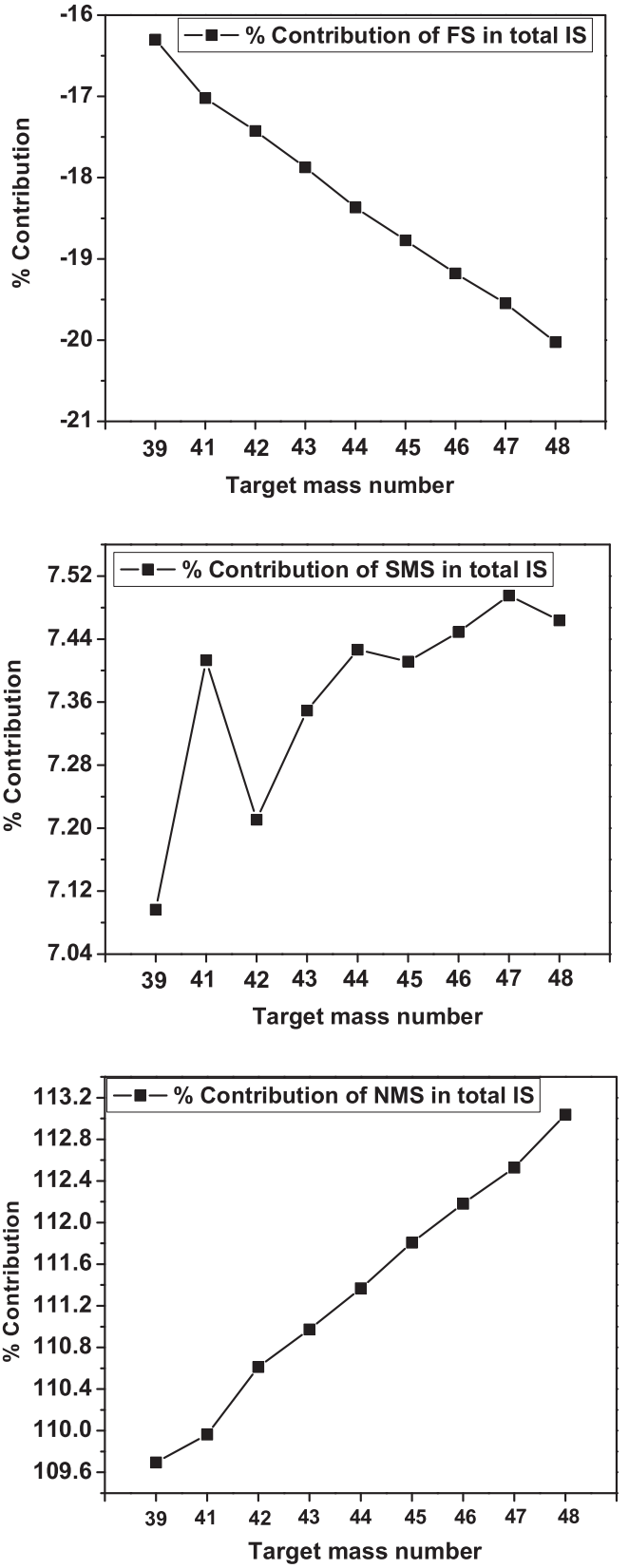

FIG. 4. Effects of the change in neutron numbers on the percent contribution of the FS, SMS, and NMS in the total isotopic shift for the D_2 line of Ca II. Here the reference isotope is Ca^{40}.

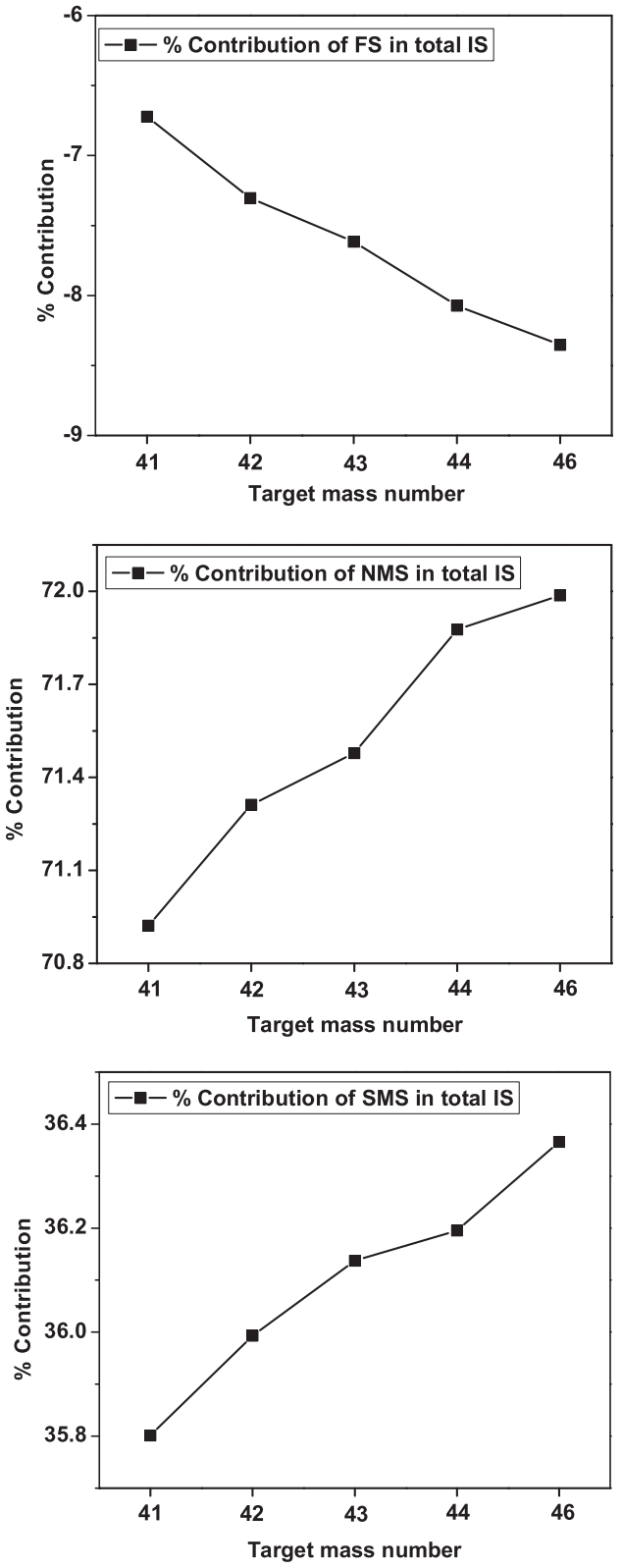

FIG. 5. Effects of the change in neutron numbers on the percent contribution of the FS, SMS, and NMS in the total isotopic shift for the D_2 line percent of Sc III. Here the reference isotope is Sc^{43}.

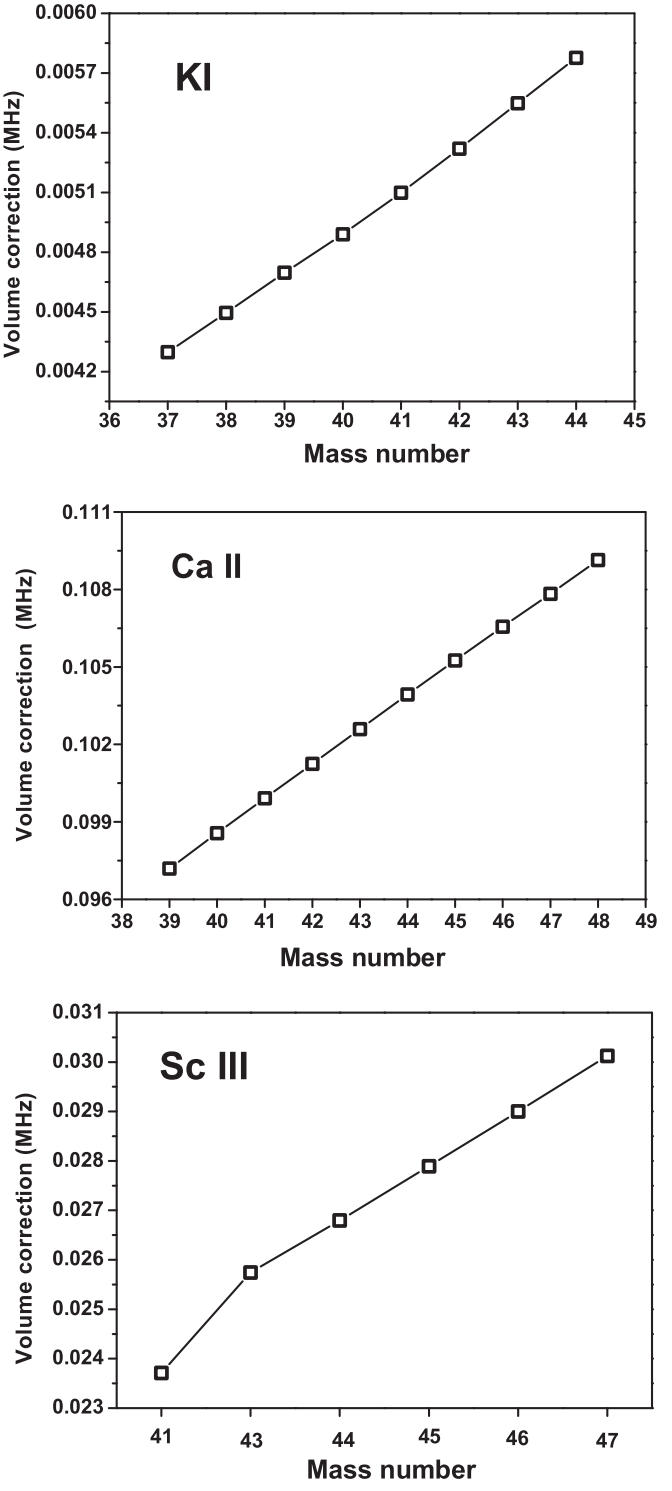

FIG. 6. Effects of the changes in nuclear volume on the $S_{1/2}$ orbital.

In Figs. 3–5, we plot percent contributions for the FS, SMS, and NMS for K I, Ca II, and Sc III, respectively. These curves show the effects of increasing neutron number differences on these three individual species of the IS for the D_2 lines. The percent contributions of both the FS and the NMS increase for each species with the increase in neutron number. For the FS, the increment is from a more $-ve$ value to a less $-ve$ value. Here the negative increment means the energy difference between $S_{1/2}$ and $P_{3/2}$ states decreases. But, if we consider the SMS along with the FS and NMS, i.e., the total IS sends the above states away from each other.

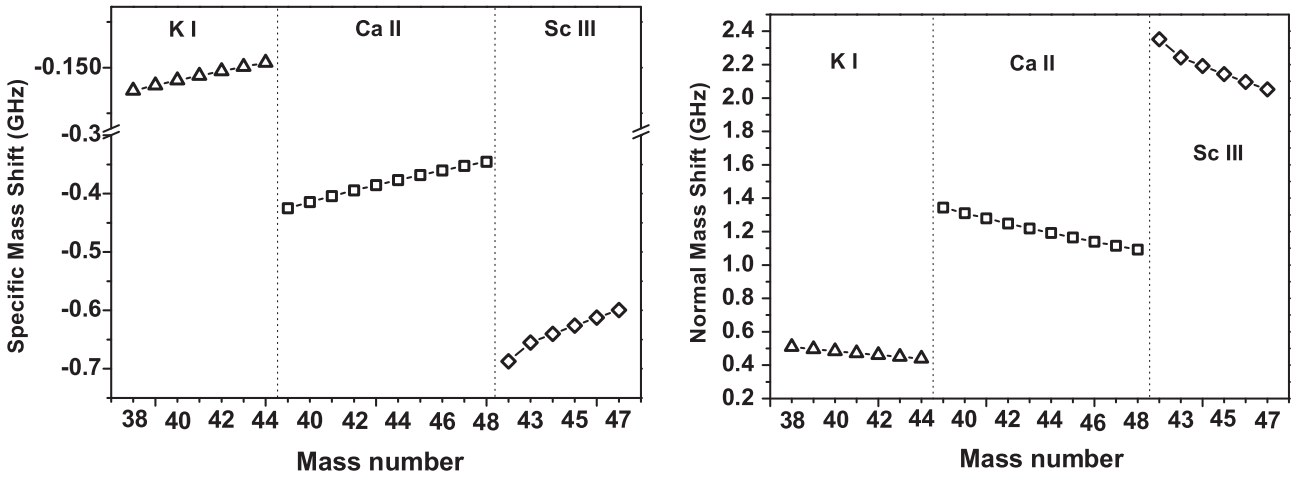

FIG. 7. Effects of increasing nuclear mass on the $S_{1/2}$ orbital.

In Figs. 6 and 7 we show the effect of increasing the neutron number on the volume and mass correction terms of the $S_{1/2}$ states, respectively, for the system concerned. We see that the volume correction of the $S_{1/2}$ level is increasing as the volume of the nucleus increases without changing its charge. However, the mass shifts are decreasing as the mass of the nucleus increases without changing the charge. It reflects the fact that the motion of the nucleus decreases with the increasing mass number. These effects are similar for the other two levels $P_{1/2}$ and $P_{3/2}$, and they are not shown in the paper.

Table VII is dedicated to examine the correlation effects on the correction terms on individual energy levels. The correction terms arise due to the change in nuclear model from a point to a finite nucleus. The DF and RCC values of the total corrections are given in separate columns in the table for each of the $S_{1/2}$, $P_{1/2}$, and $S_{3/2}$ states to study the correlation contribution. We notice that the correlations to the $S_{1/2}$ states are minimum. It can be easily observed from the table that the correlation contributions are smoothly increasing with increasing neutron numbers for all the species.

To observe the odd-even staggering (OES) phenomena in the volume correction terms we use the experimental $\delta\langle r^2\rangle^{40-A}$ of the Ca isotopes from Refs. [45,46], but due to the unavailability of the rms radius of the ^{40}Ca isotope, we consider the same from Eq. (18), given in the Theory section. OES is an empirical feature that occurs due to the existence of nuclear pairing energy [47]. It says that the binding is stronger for even isotopes than for their odd neighbors [48]. So the volume or rms radius of the nucleus of even isotopes is smaller than that for their odd neighbor isotopes, and this rms radius is directly related with the volume correction term of the atomic energy levels. Here we compare the volume correction terms of the $P_{1/2}$ states for each isotope with the arithmetic mean of the volume corrections of their two neighboring isotopes and plot them in Fig. 8(a). It is clearly seen that all the correction terms for the odd neutrons are larger than the above-stated mean values. A similar feature has been observed for the $S_{1/2}$ state. This reflects the fact that the binding energy of odd isotopes is comparatively smaller than the arithmetic mean of the binding energy of two adjacent even isotopes. This is the definition of OES [49]. According to Tomlinson III and Stroke, the spectral centroids of odd neutron isotopes stay closer to the spectral centroid of adjacent lighter isotopes with an even neutron [50]. To reestablish this definition of OES we take the direct difference of volume correction terms between two adjacent isotopes. These results are plotted in Fig. 8(b). The jig-jag curve explores the fact that the differences in corrections at each energy level between all the odd isotopes and their adjacent lightweight even isotopes are smaller than the differences with their adjacent heavy isotopes. The differences in volume correction terms for different isotopes from the isotope ^{40}Ca are plotted and obtained as the well-known [51,52] parabolic structure as shown in Fig. 8(c). This structure signifies once again the OES phenomena in volume correction terms. In all the graphs we see little different behavior of the ^{44}Ca isotope, which is already known [52] due to close-packed nuclear structure. Figure 8 has been shown here only for the $P_{1/2}$ states of the Ca II element and is true for the wave functions of other states whose contributions are significant in the nuclear region. Similar features have been observed for K I and Sc III but are not shown in this paper.

Table VIII presents the mass shift constants ($K_{\rm SMS}$ and $K_{\rm NMS}$) of the levels involved in D_1 and D_2 transitions for all four atomic systems. These have been calculated by Berengut *et al.* [10] and Safronova and Johnson [11] for some levels which are compared here. We give the DF and CC results in separate columns of the table. Our DF results for Mg II agree well with the results calculated by Berengut *et al.* Safronova and Johnson present their calculated constants where $S^{(2)}$'s are taken into account with Hartree-Fock results [10]. However our DF results are well comparable with their $P^{(1)} + S^{(2)}$ values for K I and Ca II. The CC correlations increase the absolute values of $K_{\rm SMS}$, which are negative in sign both at the DF and at the CC levels. This contradicts the correlated calculations by the other two groups for most of the states. Their calculated correlations for the $S_{1/2}$ state are larger than for the $P_{1/2}$ and $P_{3/2}$ states. For Mg II, their correlations became so large that they alter the sign of $K_{\rm SMS}$. But as expected we see that the correlation effect is minimum for the $S_{1/2}$ state in

TABLE VII. Level corrections for the IS from a point nucleus to a finite nucleus for the first three energy levels $S_{1/2}$, $P_{1/2}$, and $P_{3/2}$ of Mg II, K I, Ca II, and Sc III in units of cm^{-1}. Correction calculated at DF and CC levels. The differences between these two results give the correlation contributions.

		$nS_{1/2}$		$nP_{1/2}$		$nP_{3/2}$	
Elements	Isotopes	DF	CC	DF	CC	DF	CC
Mg II	24	2.507	2.491	1.350	1.130	1.351	1.127
	25	2.408	2.381	1.295	1.085	1.297	1.082
	26	2.317	2.270	1.245	1.027	1.247	1.025
K I	38	0.306	0.359	0.247	0.177	0.247	0.178
	39	0.298	0.351	0.240	0.173	0.241	0.174
	40	0.291	0.343	0.234	0.169	0.235	0.170
	41	0.284	0.335	0.228	0.165	0.229	0.166
	42	0.277	0.328	0.223	0.161	0.223	0.162
	43	0.271	0.321	0.218	0.158	0.218	0.159
	44	0.265	0.314	0.213	0.154	0.213	0.155
Ca II	39	0.974	1.025	0.694	0.506	0.699	0.497
	40	0.953	1.003	0.678	0.493	0.681	0.484
	41	0.934	0.982	0.661	0.481	0.664	0.472
	42	0.915	0.963	0.645	0.469	0.648	0.461
	43	0.897	0.945	0.630	0.458	0.633	0.450
	44	0.880	0.926	0.615	0.447	0.618	0.439
	45	0.864	0.909	0.601	0.437	0.604	0.429
	46	0.848	0.893	0.588	0.427	0.591	0.420
	47	0.834	0.877	0.575	0.418	0.578	0.411
	48	0.820	0.863	0.563	0.409	0.566	0.402
Sc III	41	1.629	1.706	1.225	0.862	1.234	0.847
	43	1.557	1.630	1.168	0.822	1.177	0.808
	44	1.523	1.595	1.142	0.804	1.150	0.790
	45	1.491	1.562	1.117	0.786	1.125	0.762
	46	1.461	1.530	1.093	0.769	1.100	0.756
	47	1.432	1.499	1.069	0.753	1.077	0.740

our calculation, and for most of the cases it increases absolute values of K_{SMS}. The correlation effects on K_{NMS} are much smaller than K_{SMS}. Shift constants for Sc III calculated here were not available in literature.

We compare our calculated frequency shift constants (K_{SMS} and K_{NMS}) for the D_1 and D_2 transition lines with few published results in Table IX. Berengut *et al.* [10], Safronova and Johnson [11], and Korol and Kozlov [2] have performed these calculations for Mg II using different theories, and our CC results are in good agreement with the other results. For K I and Ca II, significant differences in K_{SMS} are observed. Safronova and Johnson got positive values of K_{SMS} for both K I and Ca II, whereas we get negative values for Ca II.

IV. CONCLUSION

The isotopic shift in D_1 and D_2 transitions, level corrections, and mass constants of relevant energy levels for Mg II, K I, Ca II, and Sc III are calculated in the fully *ab initio* way using all-order highly correlated relativistic coupled-cluster theory. Some IS estimations performed here were not available in literature. We optimize all the active

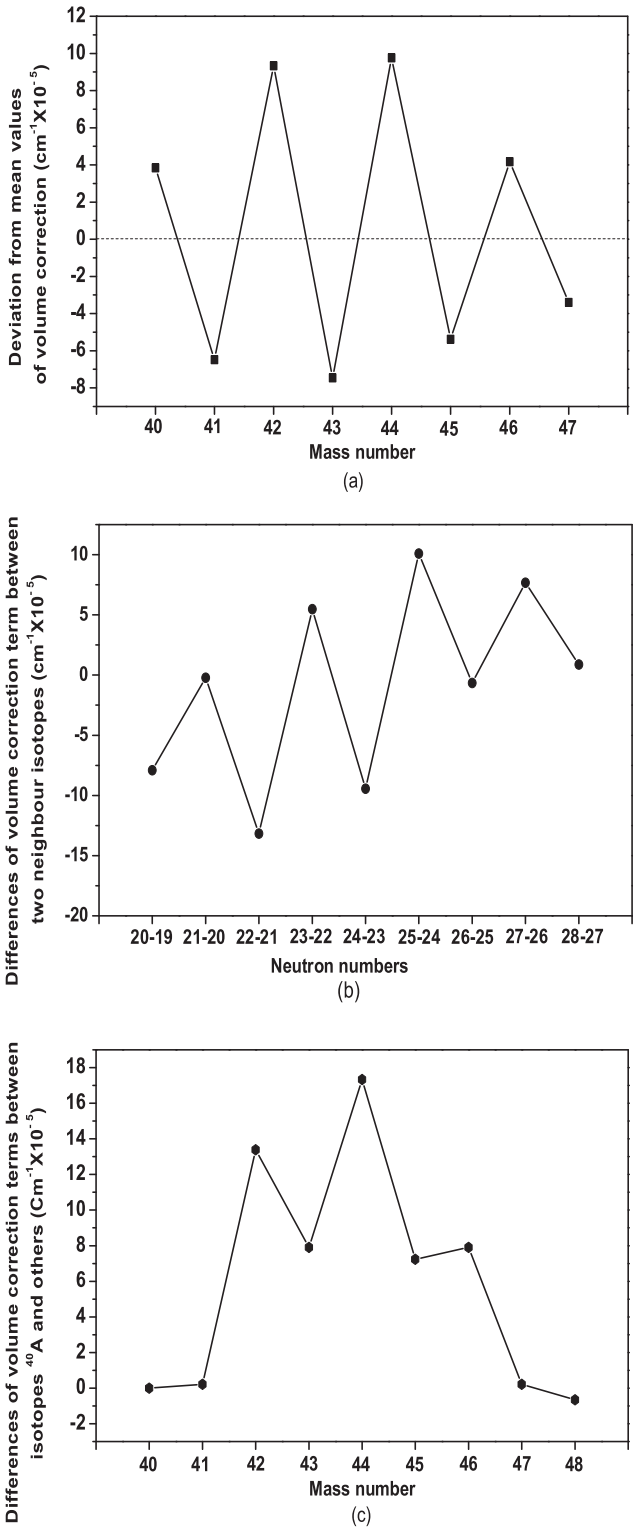

FIG. 8. In graph (a) the deviation of the volume correction terms of the $P_{1/2}$ orbitals of different Ca isotopes from the arithmetic mean of the volume correction of two adjacent isotopes are plotted here. In graph (b) we plot the differences of the volume correction terms of the same states for two adjacent isotopes, i.e., volume correction terms corresponding to the second isotope are subtracted from the same volume correction terms of the first one. We calculate the difference in volume correction terms of different isotopes with reference to ^{40}Ca and plotted in graph (c).

TABLE VIII. The mass shift constants K_{SMS} and K_{NMS} for different energy levels of the most abundant isotopes in gigahertz units and their comparisons with other calculations.

		K_{SMS}				K_{NMS}	
		DF		CC			
Isotopes	State	Ours	Others	Ours	Others	DF	CC
^{24}Mg	$3S_{1/2}$	−174.1	−171.0[a]	−206.5	83.0,[a]38.0[b]	1969.7	1982.0
	$3P_{1/2}$	−410.2	−408.0[a]	−571.6	−296.0,[a]−324.0[b]	1388.2	1393.1
	$3P_{3/2}$	−404.2	−402.0[a]	−572.1	−290.0,[a]−323.0[b]	1383.7	1391.7
^{39}K	$4S_{1/2}$	−193.0	−195.6[b]	−189.9	–74.7[b]	549.4	595.3
	$4P_{1/2}$	−66.1	−59.6[b]	−161.2	–24.7[b]	354.8	362.2
	$4P_{3/2}$	−58.1	−59.0[b]	−159.1	–24.3[b]	348.5	359.4
^{40}Ca	$4S_{1/2}$	−502.0	−506.0[b]	−505.4	–259.0[b]	1548.5	1598.6
	$4P_{1/2}$	−303.1	−290.0[b]	−535.6	–204.0[b]	1133.7	1140.6
	$4P_{3/2}$	−288.8	−286.0[b]	−538.3	–200.0[b]	1123.6	1132.9
^{45}Sc	$4S_{1/2}$	−865.7		−864.9		2859.1	3115.1
	$4P_{1/2}$	−708.9		−1210.4		2232.6	2267.6
	$4P_{3/2}$	−666.1		−1173.8		2219.6	2246.1

[a]Berengut *et al.* [10].
[b]Safronova and Johnson [11].

bound orbitals in reference states by the linear regression technique and get remarkable agreement for the IS values with the recent experimental results. Our RCC calculation for the D_2 lines of ^{24,26}Mg II and ^{25,26}Mg II achieved high accuracy, and the discrepancies are 0.36% and 0.07%, respectively. Wherever recent experiments are available, our results of the IS for K I and Ca II are well within the experimental uncertainties. It is known that relativistic corrections to the IS for the Mg II D_2 line is around 1% [2]. Also, it has been shown by Kállay *et al.* [53] that higher-order excitations of the RCC method can improve the results less than 0.01%. Therefore, the relativistic corrections and the higher-order excitations have not been considered in our calculations. In literature [54–56], there have been estimations of nuclear polarization corrections and quantum electrodynamics effects on the IS, and they are shown to be negligible for singly and doubly ionized systems. Odd-even staggering and magic neutron number effects are established in the case of volume correction calculations. Interesting cumulative features are observed compared to earlier correlation calculations of this system. We expect that our results will be helpful for α-variation calculations and the study of particle physics beyond the standard model.

ACKNOWLEDGMENTS

We are thankful to Professor B. P. Das and Dr. R. K. Choudhuri, IIA, Bangalore, India for providing the COUPLED-CLUSTER code to us and Dr. Gopal Dixit, Max-Born Institute for Non-linear Optics, Germany, for valuable suggestion. We also want to acknowledge the Board of Research in Nuclear Sciences (BRNS), India for funding.

TABLE IX. Isotope shift constants K_{SMS} and K_{NMS} of different transitions of the most abundant isotopes in gigahertz units and their comparisons with other calculations.

		K_{SMS}		K_{NMS}	
Isotopes	State	CC	Others	CC	Others
^{24}Mg	$3S_{1/2} \rightarrow 3P_{1/2}$	−365.1	–362.0,[a] –373.0(12.0),[b] –387.0[c]	−588.9	–585.6[c]
	$3S_{1/2} \rightarrow 3P_{3/2}$	−365.6	–361.0,[a] –373.0(6.0)[b] –381.0[c]	−590.4	–588.1[c]
^{39}K	$4S_{1/2} \rightarrow 4P_{1/2}$	29.7	50[a]	233.1	
	$4S_{1/2} \rightarrow 4P_{3/2}$	30.8	50.4[a]	235.9	
^{40}Ca	$4S_{1/2} \rightarrow 4P_{1/2}$	−30.2	55[a]	−453.9	
	$4S_{1/2} \rightarrow 4P_{3/2}$	−32.9	59[a]	−461.6	
^{45}Sc	$4S_{1/2} \rightarrow 4P_{1/2}$	345.5		847.5	
	$4S_{1/2} \rightarrow 4P_{3/2}$	308.9		869.0	

[a]Safronova and Johnson [11].
[b]Berengut *et al.* [10].
[c]Kozlov *et al.* [4].

[1] J. K. Webb, V. V. Flambaum, C. W. Churchill, M. J. Drinkwater, and J. D. Barrow, Phys. Rev. Lett. **82**, 884 (1999).

[2] V. A. Korol and M. G. Kozlov, Phys. Rev. A **76**, 022103 (2007).

[3] D. F. Mota and J. D. Barrow, Phys. Lett. B **581**, 141 (2004).

[4] M. G. Kozlov, V. A. Korol, J. C. Berengut, V. A. Dzuba, and V. V. Flambaum, Phys. Rev. A **70**, 062108 (2004).

[5] C. Nazé, Ph.D. thesis, Relativistic *ab initio* calculation of isotope shift, Universitas Bruxell Lensis, 2012.

[6] V. A. Dzuba, W. R. Johnson, and M. S. Safronova, Phys. Rev. A **72**, 022503 (2005).

[7] V. A. Dzuba, V. V. Flambaum, and B. Roberts, Phys. Rev. A **86**, 062512 (2012).

[8] N. N. Dutta and S. Majumder, Phys. Rev. A **90**, 012522 (2014).

[9] F. A. Parpia and A. K. Mohanty, Phys. Rev. A **46**, 3735 (1992).

[10] J. C. Berengut, V. A. Dzuba, and V. V. Flambaum, Phys. Rev. A **68**, 022502 (2003).

[11] M. S. Safronova and W. R. Johnson, Phys. Rev. A **64**, 052501 (2001).

[12] E. Gaidamauskas, C. Naźe, P. Rynkun, G. Gaigalas, P. Jönsson, and M. Godefroid, J. Phys. B: At., Mol. Opt. Phys. **44**, 175003 (2011).

[13] S. Roy, N. N. Dutta, and S. Majumder, Phys. Rev. A **89**, 042511 (2014).

[14] D. F. Feller and K. Ruedenberg, Theor. Chim. Acta **52**, 231 (1979).

[15] T. P. Harty, D. T. C. Allcock, C. J. Ballance, L. Guidoni, H. A. Janacek, N. M. Linke, D. N. Stacey, and D. M. Lucas, Phys. Rev. Let. **113**, 220501 (2014).

[16] V. Batteiger, S. Knünz, M. Herrmann, G. Saathoff, H. A. Schüssler, B. Bernhardt, T. Wilken, R. Holzwarth, T. W. Hänsch, and Th. Udem, Phys. Rev. A **80**, 022503 (2009).

[17] G. Salomon, L. Fouché, P. Wang, A. Aspect, P. Bouyer, and T. Bourdel, Europhys. Lett. **104**, 63002 (2013).

[18] N. Lehner, C. Trundle, F. P. Keenan, K. R. Sembach, and D. L. Lambert, Astron. Astrophys. **370**, 996 (2001).

[19] Y. Chmielewski, Astron. Astrophys. **353**, 666 (2000).

[20] D. K. Nandy, Y. Singh, B. K. Sahoo, and C. Li, J. Phys. B: At., Mol. Opt. Phys. **44**, 225701 (2011).

[21] M. S. Safronova and U. I. Safronova, Phys. Rev. A **85**, 022504 (2012).

[22] F. A. Parpia, M. Tong, and C. F. Fischer, Phys. Rev. A **46**, 3717 (1992).

[23] N. N. Dutta, S. Roy, G. Dixit, and S. Majumder, Phys. Rev. A **87**, 012501 (2013).

[24] W. R. Johnson, *Atomic Structure Theory*, Lectures on Atomic Physics (Springer, Berlin/Heidelberg/New York, 2006).

[25] S. Wilson, Theor. Chim. Acta **58**, 31 (1980).

[26] J. P. Vinti, Phys. Rev. **56**, 1120 (1939).

[27] J. P. Vinti, Phys. Rev. **58**, 882 (1940).

[28] I. Lindgren and J. Morrison, in *Atomic Many-Body Theory*, edited by G. E. Lambropoulos and H. Walther (Springer, Berlin, 1985), Vol. 3.

[29] W. R. Johnson and G. Soff, At. Data Nucl. Data Tables **33**, 405 (1985).

[30] D. M. Silver and W. K. Nieuntoort, Chem. Phys. Lett. **57**, 421 (1978).

[31] F. A. Parpia, C. F. Fischer, and I. P. Grant, Comput. Phys. Commun. **175**, 745 (2006).

[32] R. E. Drullinger, D. J. Wineland, and J. C. Bergquist, Appl. Phys. **22**, 365 (1980).

[33] L. G. Mundie and K. W. Meissner, Phys. Rev. **65**, 265 (1944).

[34] J. C. Pickering, A. P. Thorne, and J. K. Webb, Mon. Not. R. Astron. Soc. **300**, 131 (1998).

[35] B. K. Sahoo, J. Phys. B: At., Mol. Opt. Phys. **43**, 231001 (2010).

[36] J. K. Webb, M. T. Murphy, V. V. Flambaum, V. A. Dzuba, J. D. Barrow, C. W. Churchill, J. X. Prochaska, and A. M. Wolfe, Phys. Rev. Lett. **87**, 091301 (2001).

[37] F. Touchard, P. Guimbal, S. Büjttgenbach, R. Klapisch, M. D. S. Simon, J. M. Serre, C. Thibault, H. T. Duong, P. Juncar, S. Liberman, J. Pinard, and J. L. Vialle, Phys. Lett. B **108**, 169 (1982).

[38] N. Bendali, H. T. Duong, and J. L. Vialle, J. Phys. B: At., Mol. Phys. **14**, 4231 (1981).

[39] S. Falke, E. Tiemann, C. Lisdat, H. Schnatz, and G. Grosche, Phys. Rev. A **74**, 032503 (2006).

[40] S. Maleki and A. T. Goble, Phys. Rev. A **45**, 524 (1992).

[41] A.-M. Mårtensson-Pendrill, A. Ynnerman, H. Warston, L. Verrmeeren, R. E. Silverans, A. Klein, R. Neugart, C. Schulz, P. Lievens, and The ISOLDE Collaboration, Phys. Rev. A **45**, 4675 (1992).

[42] F. Kurth, T. Gudjons, B. Hilbert, T. Reisinger, G. Werth, and A.-M. Mårtensson-Pendrill, Z. Phys. D: At., Mol. Clusters **34**, 227 (1995).

[43] H. W. Brandt, K. Heilig, H. Knöckel, and A. Steljdel, Phys. Lett. A **64**, 29 (1977).

[44] W. Nörtershäusera, K. Blaum, K. Icker, P. Müller, A. Schmitt, K. Wendt, and B. Wiche, Eur. Phys. J. D **2**, 33 (1998).

[45] C. W. P. Palmer, P. E. G. Baird, S. A. Blundell, J. R. Brandenbergert, C. J. Foot, D. N. Stacey, and G. K. Woodgate, J. Phys. B: At., Mol. Phys. **17**, 2197 (1984).

[46] L. Vermeeren, P. Lievens, R. E. Silverans, U. Georg, M. Keim, A. Klein, R. Neugart, M. Neuroth, F. Buchinger, and the ISOLDE Collaboration, J. Phys. G: Nucl. Part. Phys. **22**, 1517 (1996).

[47] W. Satula, J. Dobaczewski, and W. Nazarewicz, Phys. Rev. Lett. **81**, 3599 (1998).

[48] W. Heisenberg, Z. Phys. **78**, 156 (1932).

[49] L. J. Wang, B. Y. Sun, J. M. Dong, and W. H. Long, Phys. Rev. C **87**, 054331 (2013).

[50] W. J. Tomlinson III and H. H. Stroke, Phys. Rev. Lett. **8**, 436 (1962).

[51] M. Avgoulea, Y. P. Gangrsky, K. P. Marinova, S. G. Zemlyanoi, S. Fritzsche, D. Iablonskyi, C. Barbieri, E. C. Simpson, P. D. Stevenson, J. Billowes, P. Campbell, B. Cheal, B. Tordoff, M. L. Bissell, D. H. Forest, M. D. Gardner, G. Tungate, J. Huikari, A. Nieminen, H. Penttilä, and J. Äystö, J. Phys. G: Nucl. Part. Phys. **38**, 025104 (2011).

[52] E. Caurier, K. Langanke, G. Martínez-Pinedo, F. Nowacki, and P. Vogel, Phys. Lett. B **522**, 240 (2001).

[53] M. Kállay, H. S. Nataraj, B. K. Sahoo, B. P. Das, and L. Visscher, Phys. Rev. A **83**, 030503 (2011).

[54] N. A. Zubova, Y. S. Kozhedub, V. M. Shabaev, I. I. Tupitsyn, A. V. Volotka, G. Plunien, C. Brandau, and T. Stohlker, Phys. Rev. A **90**, 062512 (2014).

[55] M. Puchalski, A. M. Moro, and K. Pachucki, Phys. Rev. Lett. **97**, 133001 (2006).

[56] Z.-C. Yan and G. W. F. Drake, Phys. Rev. Lett. **91**, 113004 (2003).

[57] R. Bruch, K. Heilig, and D. Wendlant, in *Proceedings of the International Conference on Optical Pumping and Atomic Line Shape, Warsaw, 1968*, edited by T. Skalinski (Panstwowe Wydawn, Warsaw, 1968), p. 299.